J. Fluid Mech. (2014), *vol.* 756, *pp.* 89–109.

doi:10.1017/jfm.2014.348

Heat transport and pressure buildup during carbon dioxide injection into depleted gas reservoirs

Simon A. Mathias†, Jim N. McElwaine and Jon G. Gluyas

Department of Earth Sciences, Durham University, Durham DH1 3LE, UK

(Received 10 March 2014; revised 9 June 2014; accepted 15 June 2014)

In this article, a two-layer vertical equilibrium model for the injection of carbon dioxide into a low-pressure porous reservoir containing methane and water is developed. The dependent variables solved for include pressure, temperature and CO_2–CH_4 interface height. In contrast to previous two-layer vertical equilibrium models in this context, the compressibility of all material components is fully accounted for. Non-Darcy effects are also considered using the Forchheimer equation. The results show that, for a given injection scenario, as the initial pressure in the reservoir decreases, both the pressure buildup and temperature change increase. A comparison was conducted between a fully coupled non-isothermal numerical model and a simplified model where fluid properties are held constant with temperature. This simplified model was found to provide an excellent approximation when using the injection fluid temperature for calculating fluid properties, even when the injection fluid was as much as $\pm 15\,^{\circ}C$ of the initial reservoir temperature. The implications are that isothermal models can be expected to provide useful estimates of pressure buildup in this context. Despite the low viscosity of CO_2 at the low pressures studied, non-Darcy effects were found to be of negligible concern throughout the sensitivity analysis undertaken. This is because the CO_2 density is also low in this context. Based on these findings, simplified analytic solutions are derived, which accurately calculate both the pressure buildup and temperature decline during the injection period.

Key words: geophysical and geological flows, low-Reynolds-number flows, porous media

1. Introduction

The potential for storing carbon dioxide (CO_2) in geological reservoirs continues to attract the attention of national greenhouse gas emission reduction strategies around the world. Reservoir types under consideration include saline aquifers, depleted oil reservoirs and depleted gas reservoirs. Saline aquifers have the advantage of being ubiquitous across the world (Bentham & Kirby 2005). However, depleted oil and gas reservoirs are often heralded due to advantages associated with better levels of

† Email address for correspondence: s.a.mathias@durham.ac.uk

current characterization (as a result of previous oil and gas production) and reduced uncertainty associated with the cap-rock integrity – the trap mechanism has already been demonstrated through the presence of hydrocarbon product originally deposited millions of years earlier (Loizzo *et al.* 2009). Many depleted gas reservoirs have the added advantage of exceptionally low abandonment pressures along with highly compressible formation fluids (gas as opposed to oil and water). Estimated CO_2 storage capacities for depleted gas reservoirs have been found to be as much as 13 times higher than those estimated for saline aquifers of equivalent geometries (Barrufet, Bacquet & Falcone 2010).

Gas reservoirs within the UK continental shelf are typically located between 700 and 3600 m below sea level (Gluyas & Hichens 2003). Reservoir net thicknesses range from 20 to 300 m, with gas saturations, fairly uniformly distributed within the reservoir units, representing between 50 and 85 % of the available pore space (Gluyas & Hichens 2003). The remainder of the pore space is generally filled with residually trapped brine. Reservoir geometries vary considerably, with the most common being domes or gently tilted slabs, covering regions of up to 250 km^2 (Gluyas & Hichens 2003).

Prior to production, gas reservoirs typically exhibit pressures at or above hydrostatic pressure (generally greater than 10 MPa). Many such reservoirs are highly compartmentalized, exhibiting poor levels of aquifer influx. Consequently, at abandonment, reservoir pressures are often found to be close to atmospheric conditions. Around the world, gas reservoir abandonment pressures commonly range between 0.35 and 0.8 MPa (MacRoberts 1962; Okwananke, Yekeen Adeboye & Sulaimon 2011). Note that, in compartmentalized reservoirs, gas saturations tend to change very little following reservoir depletion, owing to the increase in gas volume associated with the pressure decline.

A number of recent simulation studies have discussed the interesting thermal effects that develop as a consequence of CO_2 injection into geological reservoirs. These include cooling due to expansion, heating due to compression, heating and cooling due to dissolution and vaporization, respectively, differences in temperature associated with injection and reservoir fluids, and heating due to viscous heat dissipation (Oldenberg 2007; Andre, Azaroual & Menjoz 2010; Han *et al.* 2010). Owing to the Joule–Thomson coefficient of CO_2 being larger at lower pressures, such processes are likely to be of greater significance in low-pressure depleted gas reservoirs as opposed to hydrostatic or overpressured saline aquifers (Mathias *et al.* 2010).

Most previous simulation work relating to CO_2 storage has focused on pressures greater than 10 MPa (e.g. Andre *et al.* 2010; Mathias *et al.* 2013*a*). Exceptions to these include Han *et al.* (2012), who considered a minimum initial pressure of 6.89 MPa, Ziabaksh-Ganji & Kooi (2014), who assumed an initial pressure of 6 MPa, Afanasyev (2013), who assumed a minimum initial pressure of 4.5 MPa, and Singh, Goerke & Kolditz (2011) and Singh *et al.* (2012), who considered an initial pressure of 4 MPa. However, depleted gas reservoirs are often abandoned at pressures lower than 1 MPa. Mukhopadhyay, Yang & Yeh (2012) presented numerical simulations concerning CO_2 injection into a depleted gas reservoir at 0.5 MPa. However, they ignored thermal effects and considered the reservoir to be of infinite extent. This study seeks to explore the importance of heat transport coupling on pressure buildup estimation during CO_2 injection in low-pressure depleted gas reservoirs. Furthermore, non-Darcy effects associated with high velocities around the injection well are incorporated using the Forchheimer equation.

Significant temperature changes are most likely to occur when pressure gradients (in time and space) are sharpest. This will mostly be the case during the injection

period. Consequently, although many previous CO_2 storage studies have studied the long periods of time after CO_2 injection has ceased (e.g. Hesse *et al.* 2007; Hesse, Orr & Tchelepi 2008; MacMinn, Szulczewski & Juanes 2010, 2011), here it is pertinent only to consider the time prior to injection ceasing.

The outline of this article is as follows. Firstly, the governing equations concerning mass conservation are presented for a system whereby pure CO_2 is injected into a low-pressure closed reservoir containing methane (CH_4) and residually trapped water. Expressions for vertically integrated fluxes are derived following the adoption of the Forchheimer equation along with an assumption of vertical equilibrium. A corresponding energy conservation statement is presented. Details of the solution procedure are provided followed by details concerning the obtaining of relevant thermodynamic properties. Further insight is then sought by deriving simplified analytic solutions for heat transport and pressure buildup. A sensitivity analysis is then conducted to explore the role of initial pressure and heat flow coupling on pressure buildup during CO_2 injection into low-pressure depleted gas reservoirs. Finally the article summarizes and concludes.

2. The mathematical model

Consider a fully penetrating vertical injection well of radius r_w [L] located at the centre of a horizontally oriented, homogeneous and isotropic, confined cylindrical reservoir of thickness H [L] and radial extent r_e [L]. Four material components are considered and referenced by the subscript i, which takes the values c for CO_2, m for CH_4, w for water and r for rock. A mixture theory is assumed such that all components are considered to exist at every point in space with some volume fraction θ_i. The four material components must satisfy the volume constraint $\sum_i \theta_i = 1$.

The reservoir is initially filled with CH_4 alongside a uniform residual saturation of water with volume fraction θ_w [–]. The H_2O is assumed to be residually trapped and immobile such that $\theta_w \rho_w$ is constant (Singh *et al.* 2011, 2012). The volume fraction of the rock is $\theta_r = 1 - \phi$, where ϕ [–] is the porosity, and the product $\theta_r \rho_r$ is also constant. The compressibility of all components is allowed for, although, as shown later, in the context of this study, the compressibility and thermal expansion of the water and rock are negligible owing to the relatively small pressure and temperature changes involved.

The CO_2 is injected at the origin at a constant mass flow rate M_0 [$\mathrm{M\,T^{-1}}$]. Although the CO_2 and CH_4 are miscible (Ren *et al.* 2000), for simplicity, dispersion and mixing of the two components are ignored and a sharp interface is assumed, located at an elevation of h_c [L] above the base of the reservoir (similar to Nordbotten & Celia 2006). At 35 °C, for pressures ranging between 0.7 and 15 MPa, the densities of CO_2 and CH_4 are in the ranges 12–815 kg $\mathrm{m^{-3}}$ and 4–111 kg $\mathrm{m^{-3}}$, respectively (Lemmon, McLinden & Friend 2013). The ranges of the corresponding dynamic viscosities for CO_2 and CH_4 are 15.5–73.6 μPa s and 11.6–16.2 μPa s, respectively (Lemmon *et al.* 2013). Because the CO_2 is denser than the CH_4, h_c represents the thickness of the CO_2 layer. The thickness of the CH_4 layer is then $h_m = H - h_c$.

Let us denote $P(r, t)$ [$\mathrm{M\,L^{-1}\,T^{-2}}$] and $T(r, t)$ [Θ^{-1}] as the pressure and temperature at the location of the CO_2–CH_4 interface, respectively, where r [L] is the horizontal radial distance from the centre of the injection well and t [T] is time after commencement of injection.

In most cases of physical interest, $r_e \gg H$, so it is convenient to make a shallowness assumption (Nordbotten & Celia 2006; Hesse *et al.* 2007, 2008; MacMinn *et al.*

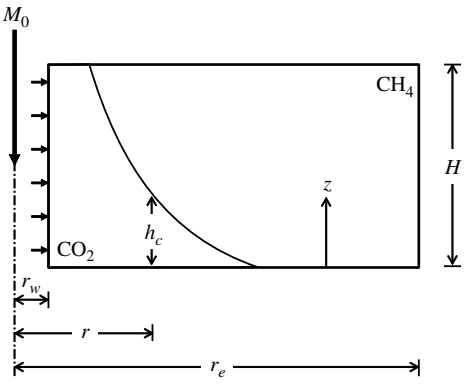

FIGURE 1. Schematic diagram of conceptual model.

2010, 2011). This can be rigorously derived as an expansion in $H/r_e \ll 1$, but the result is equivalent to assuming vertical equilibrium. It is therefore assumed that the temperature is uniform vertically and identical in the rock, CO_2, CH_4 and water. The densities ρ_i [$\mathrm{M\,L^{-3}}$] for each fluid species are also assumed to be constant vertically and given by the equation of state evaluated at the interface, that is, using P and T. The vertical momentum equation is then simplified by assuming an equilibrium between gravity and hydrostatic pressure such that (Hesse *et al.* 2007)

$$P(r, z, t) = \begin{cases} P(r, t) + \rho_c g(h_c - z), & 0 \leqslant z \leqslant h_c, \\ P(r, t) + \rho_m g(h_c - z), & h_c < z \leqslant H, \end{cases} \tag{2.1}$$

where P [$\mathrm{M\,L^{-1}\,T^{-2}}$] is the local pressure, ρ_c [$\mathrm{M\,L^{-3}}$] and ρ_m [$\mathrm{M\,L^{-3}}$] are the densities of CO_2 and CH_4, respectively, g [$\mathrm{L\,T^{-2}}$] is gravitational acceleration and z [L] is the height above the base of the reservoir. After depth integrating, the primary dependent variables of our model then become $P(r, t)$, $T(r, t)$ and $h_c(r, t)$. Some general features of the conceptual model are illustrated further in figure 1.

Note that, by assuming the fluids are incompressible, ignoring heat transport and temperature changes, and ignoring the density difference between the different components, such a problem reduces to the classic equation of Buckley & Leverett (1942), where relative permeability is assumed to be a linear function of h_c and h_c is equivalent to fluid saturation.

2.1. *Mass conservation*

The depth-integrated mass conservation equation for the CO_2 and CH_4 can be written as

$$\frac{\partial}{\partial t}(\theta_i \rho_i h_i) = -\frac{1}{r}\frac{\partial}{\partial r}(r \rho_i Q_i) \equiv R_i, \tag{2.2}$$

where R_i [$\mathrm{M\,L^{-2}\,T^{-1}}$] denotes the right-hand side of (2.2) and the vertically integrated volume fluxes Q_i [$\mathrm{L^2\,T^{-1}}$] are defined as

$$Q_c = \int_0^{h_c} q_c \,\mathrm{d}z \quad \text{and} \quad Q_m = \int_{h_c}^{H} q_m \,\mathrm{d}z, \tag{2.3a,b}$$

and q_i [$\mathrm{L\,T^{-1}}$] are the respective volume fluxes.

2.1.1. *Determination of the vertically integrated volume fluxes*

Volume fluxes, in the context of simulating CO_2 storage problems, are generally calculated using Darcy's law. However, owing to the lower dynamic viscosity of CO_2 at the relevant pressures of concern, it is pertinent to consider non-Darcy losses using the Forchheimer equation (Zeng & Grigg 2006). Therefore, the fluxes q_i are defined by the Forchheimer equation

$$\frac{\mu_i q_i}{k k_{rg}} + \rho_i b q_i |q_i| + \frac{\partial P}{\partial r} = 0, \qquad \begin{array}{ll} 0 \leqslant z \leqslant h_c & \text{when } i = c, \\ h_c < z \leqslant H & \text{when } i = m, \end{array} \tag{2.4}$$

where k [L^2] is the reservoir permeability, k_{rg} [–] is the relative permeability of the gas, which is treated as uniform and constant, b [L^{-1}] is the Forchheimer coefficient and μ_i [$M\,L^{-1}\,T^{-1}$] are the dynamic viscosities of CO_2 and CH_4. Denoting $J = \partial P/\partial r < 0$, the appropriate positive real root can be written as

$$q_i = -\frac{k k_{rg}}{\mu_i}\left(\frac{2J}{1 + (1 - \epsilon_i J)^{1/2}}\right), \tag{2.5}$$

where

$$\epsilon_i = 4\rho_i b \left(\frac{k k_{rg}}{\mu_i}\right)^2. \tag{2.6}$$

A Maclaurin series expansion about small $\epsilon_i J$ leads to

$$q_i = -[1 + \epsilon_i J/4 + O(\epsilon_i^2 J^2)]\frac{k k_{rg} J}{\mu_i}, \tag{2.7}$$

from which it can be seen that the accuracy of the Darcy approximation is given by the size of the non-dimensional group $\epsilon_i J$. The issue for radially divergent (and convergent) flow problems is that J becomes very large as one approaches the origin (the injection well in this case). Therefore, it is not clear whether non-Darcy effects can be ignored from information about ϵ_i alone.

Note that the uniform relative permeability values, k_{rg}, assumed for CO_2 and CH_4 are equivalent to the end-point relative permeability for gas in a two-phase relative permeability function, k_{rg0} [–] (e.g. Mathias *et al.* 2013*a*). In this article, for simplicity, CO_2 and CH_4 are assumed to have the same relative permeabilities. In reality, they may have different relative permeabilities due to differences in interfacial tension (IFT) and contact angle associated with CO_2–brine and CH_4–brine mixtures. Bachu & Bennion (2008*a*) observed a set of k_{rg0} values for the same sandstone core, ranging from 0.298 to 0.526, for CO_2–brine mixtures, with IFT ranging from 56.2 to 19.8 mN m^{-1}, respectively (IFT was varied by increasing the fluid pressure from 1.378 to 20 MPa). At 40 °C and 1 MPa of pressure, the IFT for CO_2–water and CH_4–water mixtures are around 90.95 mN m^{-1} (Bachu & Bennion 2008*b*) and 69.06 mN m^{-1} (Ren *et al.* 2000), respectively. Therefore, the relative permeabilities for CO_2–brine and CH_4–brine mixtures can be expected to be quite different. However, ignoring this difference is unlikely to significantly affect the main findings discussed hereafter.

The system is assumed to be initially free of CO_2. Fluid pressure is assumed initially uniform in the radial direction, at a value of P_0 at the base of the reservoir. The reservoir is confined on all sides by impermeable boundaries. Following, among others, Oldenberg (2007), Mathias *et al.* (2009), Han *et al.* (2010) and Mukhopadhyay

et al. (2012), a constant mass flux of pure CO_2 is applied at the injection well boundary. Such conditions are described mathematically as follows:

$$\left.\begin{array}{lll} h_c = 0, & r_w \leqslant r \leqslant r_e, & t = 0, \\ P = P_0, & r_w \leqslant r \leqslant r_e, & t = 0, \\ Q_c = M_0/(2\pi r_w \rho_c), & r = r_w, & t > 0, \\ Q_m = 0, & r = r_w, & t > 0, \\ Q_c = 0, & r = r_e, & t > 0, \\ Q_m = 0, & r = r_e, & t > 0, \end{array}\right\} \tag{2.8}$$

where P_0 [$\mathrm{M\,L^{-1}\,T^{-2}}$] is the initial pressure at the base of the reservoir.

Differentiating (2.1) with respect to r gives

$$J \equiv \frac{\partial P}{\partial r} = \begin{cases} \dfrac{\partial}{\partial r}(P + \rho_c g h_c) - gz\dfrac{\partial \rho_c}{\partial r}, & 0 \leqslant z \leqslant h_c, \\ \dfrac{\partial}{\partial r}(P - \rho_m g h_m) - gz\dfrac{\partial \rho_m}{\partial r}, & h_c < z \leqslant H, \end{cases} \tag{2.9}$$

showing that J is a linear function of z given the shallowness assumption that the fluid densities are uniform with depth. The flux (2.5) can then be substituted into (2.3) and integrated to give

$$Q_i = -\frac{h_i k k_{rg}}{\mu_i}\left[\frac{(1-\epsilon_i J_{i2})^{3/2} - (1-\epsilon_i J_{i1})^{3/2}}{3\epsilon_i^2 (J_{i2} - J_{i1})/4} + \frac{2}{\epsilon_i}\right], \tag{2.10}$$

where

$$\left.\begin{array}{ll} J_{c1} = \dfrac{\partial}{\partial r}(P + \rho_c g h_c), & J_{c2} = J_{c1} - g h_c \dfrac{\partial \rho_c}{\partial r}, \\ J_{m1} = \dfrac{\partial}{\partial r}(P - \rho_m g h_m) - g h_c \dfrac{\partial \rho_m}{\partial r}, & J_{m2} = J_{m1} - g h_m \dfrac{\partial \rho_m}{\partial r}. \end{array}\right\} \tag{2.11}$$

As written in (2.10), these fluxes appear singular for $\epsilon_i = 0$. However, further rearranging reveals that

$$Q_i = -\frac{h_i k k_{rg}}{\mu_i}\left(\frac{X_{i2} - X_{i1}}{J_{i2} - J_{i1}}\right), \quad X_{ij} = \frac{J_{ij}^2(1 - 4\epsilon_i J_{ij}/3)}{(1-\epsilon_i J_{ij})^{3/2} + 1 - 3\epsilon_i J_{ij}/2}, \quad j = 1, 2. \tag{2.12a,b}$$

Also note that for slightly compressible fluids (i.e. where fluid properties do not change much with space and time), $J_{i2} - J_{i1} \to 0$, and (2.12) can be expanded to obtain

$$Q_i = -\frac{h_i k k_{rg}}{\mu_i}\left\{\frac{2J_{iA}}{1 + (1-\epsilon_i J_{iA})^{1/2}} + \frac{J_{iB}}{(1-\epsilon_i J_{iA})^{1/2}}\left[\frac{\Upsilon_i}{12} + \frac{\Upsilon_i^3}{64} + O(\Upsilon_i^5)\right]\right\}, \tag{2.13}$$

where

$$J_{iA} = \frac{J_{i2} + J_{i1}}{2}, \quad J_{iB} = \frac{J_{i2} - J_{i1}}{2} \quad \text{and} \quad \Upsilon_i = \frac{\epsilon_i J_{iB}}{1 - \epsilon_i J_{iA}}. \tag{2.14a–c}$$

2.2. *Recasting in terms of the primary dependent variables*

The left-hand side of (2.2) can be expanded in terms of the primary dependent variables of our model, P, T and h_c, such that

$$\theta_i\rho_i h_i\left[\left(\frac{1}{\theta_i}\frac{\partial\theta_i}{\partial P}+\frac{1}{\rho_i}\frac{\partial\rho_i}{\partial P}\right)\frac{\partial P}{\partial t}+\left(\frac{1}{\theta_i}\frac{\partial\theta_i}{\partial T}+\frac{1}{\rho_i}\frac{\partial\rho_i}{\partial T}\right)\frac{\partial T}{\partial t}+\frac{1}{h_i}\frac{\partial h_i}{\partial h_c}\frac{\partial h_c}{\partial t}\right]=R_i, \tag{2.15}$$

where

$$\frac{\partial h_i}{\partial h_c}=\begin{cases}1, & i=c,\\ -1, & i=m.\end{cases} \tag{2.16}$$

Imposing the constraints that the products $\theta_w\rho_w$ and $\theta_r\rho_r$ are constant and that $\sum_i\theta_i=1$, it can be shown that, for $i=c$ or m,

$$\frac{\partial\theta_i}{\partial P}=\frac{\theta_w}{\rho_w}\frac{\partial\rho_w}{\partial P}+\frac{\theta_r}{\rho_r}\frac{\partial\rho_r}{\partial P}\quad\text{and}\quad\frac{\partial\theta_i}{\partial T}=\frac{\theta_w}{\rho_w}\frac{\partial\rho_w}{\partial T}+\frac{\theta_r}{\rho_r}\frac{\partial\rho_r}{\partial T}. \tag{2.17a,b}$$

Now consider an isothermal compressibility α_i $[\mathrm{M}^{-1}\,\mathrm{L}\,\mathrm{T}^2]$ and an isobaric expansivity β_i $[\Theta^{-1}]$ for each of the four material components, defined as

$$\alpha_i=\frac{1}{\rho_i}\left(\frac{\partial\rho_i}{\partial P}\right)_T\quad\text{and}\quad\beta_i=-\frac{1}{\rho_i}\left(\frac{\partial\rho_i}{\partial T}\right)_P, \tag{2.18a,b}$$

such that substitution of (2.17) into (2.15) leads to

$$\rho_i\left[h_i\left(\alpha_{Ei}\frac{\partial P}{\partial t}-\beta_{Ei}\frac{\partial T}{\partial t}\right)+\theta_i\frac{\partial h_i}{\partial h_c}\frac{\partial h_c}{\partial t}\right]=R_i, \tag{2.19}$$

where

$$\alpha_{Ei}=\theta_i\alpha_i+\theta_w\alpha_w+\theta_r\alpha_r\quad\text{and}\quad\beta_{Ei}=\theta_i\beta_i+\theta_w\beta_w+\theta_r\beta_r. \tag{2.20a,b}$$

2.3. *Energy conservation*

As mentioned above, pressure is assumed to be in a vertical equilibrium, whilst the temperature and fluid properties are assumed to be vertically uniform. Consequently, heat transport is a one-dimensional process. An appropriate statement of energy conservation can therefore (see chapter 2 of Nield & Bejan 2006) be written as

$$\begin{aligned}\rho_E c_{pE}\frac{\partial T}{\partial t}-\beta_E T\frac{\partial P}{\partial t}\;=\;&\frac{1}{r}\frac{\partial}{\partial r}\left(r\kappa_E\frac{\partial T}{\partial r}\right)-\left(\frac{\rho_c c_{pc}Q_c+\rho_m c_{pm}Q_m}{H}\right)\frac{\partial T}{\partial r}\\&+\left[\frac{(T\beta_c-1)Q_c+(T\beta_m-1)Q_m}{H}\right]\frac{\partial P}{\partial r}\equiv R_e,\end{aligned} \tag{2.21}$$

where R_e $[\mathrm{M}\,\mathrm{L}^{-1}\,\mathrm{T}^{-3}]$ is used to denote the right-hand side of (2.21) and

$$\left.\begin{aligned}\rho_E c_{pE}&=\theta_c'\rho_c c_{pc}+\theta_m'\rho_m c_{pm}+\theta_w\rho_w c_{pw}+\theta_r\rho_r c_{pr},\\ \beta_E&=\theta_c'\beta_c+\theta_m'\beta_m+\theta_w\beta_w+\theta_r\beta_r,\\ \kappa_E&=\theta_c'\kappa_c+\theta_m'\kappa_m+\theta_w\kappa_w+\theta_r\kappa_r,\end{aligned}\right\} \tag{2.22}$$

with c_{pi} [$\mathrm{L}^2\,\mathrm{T}^{-2}\,\Theta^{-1}$], β_i [Θ^{-1}] and κ_i [$\mathrm{M}\,\mathrm{L}\,\mathrm{T}^{-3}\,\Theta^{-1}$] being the constant-pressure specific heat capacity, thermal expansivity and thermal conductivity for the four material components, respectively, and $\theta_c' = \theta_c h_c/H$ and $\theta_m' = \theta_m h_m/H$ are the depth-weighted volume fractions for the CO_2 and CH_4, respectively.

Note that the -1 in the $(T\beta_i - 1)Q_i$ terms in (2.21) comes about due to shear heating associated with fluid movement. See chapter 2 of Nield & Bejan (2006) for further discussion on this matter.

Also note that the expression for κ_E represents a significant overestimate of the conductivity for this composite medium. For further discussion concerning effective conductivity estimation, the reader is directed to the work of Zimmerman (1989). However, even with this upper bound estimate, conduction has been found to be of negligible effect in this context.

The initial and boundary conditions are

$$\left.\begin{array}{lll} T = T_0, & r_w \leqslant r \leqslant r_e, & t = 0, \\ T = T_w, & r = r_w, & t > 0, \\ \partial T/\partial r = 0, & r = r_e, & t > 0, \end{array}\right\} \tag{2.23}$$

where T_0 [Θ] is the vertically averaged initial temperature of the reservoir and T_w [Θ] is the temperature of the injection fluid.

2.4. *Solution by method of lines*

Equations (2.19) and (2.21) now form a set of three first-order quasi-linear parabolic partial differential equations (PDEs) that can be written as

$$\begin{pmatrix} \rho_c h_c \alpha_{Ec} & -\rho_c h_c \beta_{Ec} & \theta_c \rho_c \\ \rho_m h_m \alpha_{Em} & -\rho_m h_m \beta_{Em} & -\theta_m \rho_m \\ -\beta_E T & \rho_E c_{pE} & 0 \end{pmatrix} \begin{pmatrix} \dfrac{\partial P}{\partial t} \\ \dfrac{\partial T}{\partial t} \\ \dfrac{\partial h_c}{\partial t} \end{pmatrix} = \begin{pmatrix} R_c \\ R_m \\ R_e \end{pmatrix}. \tag{2.24}$$

Equation (2.24) represents a set of three linear equations in the time derivative of the primary variables P, T and h_c, which can be solved to give an equation for each time derivative separately provided that the Jacobian does not vanish, which does not occur for $0 < h_c < H$. A method of lines approach is adopted, using a first-order backward difference spatial discretization and integrating the resulting set of ordinary differential equations (ODEs) with respect to time using the MATLAB ODE solver, ODE15s. A similar approach was previously adopted by Mathias, Butler & Zhan (2008), Mathias *et al.* (2009).

2.5. *Fluid and rock properties*

Because interactions between the CO_2, CH_4 and H_2O are ignored, only pure-component fluid properties are required. These can be obtained using the National Institute of Standards and Technology's online *NIST Chemistry WebBook* developed by Lemmon *et al.* (2013). Parameters available from the web book include ρ_i, c_{pi}, μ_i and κ_i, in addition to the constant-volume specific heat capacity c_{Vi} [$\mathrm{L}^2\,\mathrm{T}^{-2}\,\Theta^{-1}$] and the Joule–Thomson coefficient μ_{JTi} [$\mathrm{M}^{-1}\,\mathrm{L}\,\mathrm{T}^2\,\Theta$]. Invoking the Maxwell relations, the

compressibility α_i and thermal expansivity β_i can be obtained from (Cengel & Boles 2002)

$$\alpha_i = \frac{T\beta_i^2}{\rho_i(c_{pi} - c_{vi})} \quad \text{and} \quad \beta_i = \frac{\rho_i c_{pi}\mu_{JTi} + 1}{T}. \tag{2.25a,b}$$

Intensive lookup tables can be developed for the three fluids for a wide range of temperatures and pressures, prior to running the numerical model. These can then be linearly interpolated within the ODE solver during simultaneous solution of the aforementioned PDEs.

Thermal properties of the reservoir formation are taken from Oldenberg (2007) where available. These include density $\rho_r = 2600$ kg m^{-3}, constant-pressure specific heat capacity $c_{pr} = 1000$ J kg^{-1} K^{-1} and thermal conductivity $\kappa_r = 2.51$ W m^{-1} K^{-1}. A volumetric thermal expansivity of $\beta_r = 39 \times 10^{-6}$ K^{-1} is assumed, based on the linear thermal expansion coefficient (TEC) value provided for a water-saturated Berea sandstone in table IV-2 of Somerton (1992) (see also Somerton, Janah & Ashqar 1981) – note that the volumetric TEC is three times the linear TEC (see e.g. Zimmerman 2000).

Typically, rock compressibility is parametrized by a coefficient $c_r = (\theta_r - 1)^{-1} \times (\mathrm{d}\theta_r/\mathrm{d}P)_T$ (e.g. Chen, Huan & Ma 2006). However, in the current situation, the rock compressibility is defined as $\alpha_r = \rho_r^{-1}(\mathrm{d}\rho_r/\mathrm{d}P)_T$. Given that the rock is static, the product $\theta_r\rho_r$ must be a constant. Therefore, it can be shown that $\alpha_r = (1 - \theta_r)\theta_r^{-1}c_r$. Mathias *et al.* (2011*a*) previously assumed $\theta_r = 0.8$ and $\alpha_r = 4.5 \times 10^{-10}$ Pa^{-1}. This corresponds to a value of $\alpha_r = 1.125 \times 10^{-10}$ Pa^{-1}.

3. Analytic solutions

3.1. *Heat transport*

The above problem refers to a system whereby CO_2 displaces CH_4. However, the thermal front resulting from CO_2 injection is generally behind the CO_2–CH_4 interface as a result of heat retardation associated with the specific capacity of the host rock and residually trapped water. Furthermore, although there are large changes in pressure resulting from the injection process, for constant mass injection rates, these mostly occur at the beginning of injection (cf. Mathias *et al.* 2011*a*). Consequently, when considering the development of analytical solutions for heat transport in this context, Mathias *et al.* (2010) argue that one can additionally assume that (i) the presence of the CH_4 can be ignored and (ii) the pressure distribution is steady state. For mathematical tractability, Mathias *et al.* (2010) further assume the fluid properties to be constant and uniform, and that heat conduction is negligible. In this way, (2.21) reduces to

$$(\theta_c\rho_c c_{pc} + \theta_w\rho_w c_{pw} + \theta_r c_{pr})\frac{\partial T}{\partial t} = \rho_c q_c c_{pc}\left(\mu_{JTc}\frac{\partial P}{\partial r} - \frac{\partial T}{\partial r}\right) \tag{3.1}$$

and the profile for q_c becomes

$$q_c = \frac{M_0}{2\pi H\rho_c r}. \tag{3.2}$$

Substituting (2.4) into (3.1) then leads to

$$\frac{\partial T_D}{\partial \tau} + \frac{\partial T_D}{\partial \xi} = -\frac{1}{2\xi} - \frac{b_D}{(2\xi)^{3/2}} \tag{3.3}$$

subject to the initial and boundary conditions

$$\left.\begin{array}{lll} T_D = 0, & \xi > 1/2, & t_D = 0, \\ T_D = T_{wD}, & \xi = 1/2, & t_D > 0, \end{array}\right\} \tag{3.4}$$

where

$$\tau = \frac{M_0 c_{pc} t}{2\pi H r_w^2 (\theta_c \rho_c c_{pc} + \theta_w \rho_w c_{pw} + \theta_r c_{pr})}, \tag{3.5}$$

$$\xi = \frac{1}{2}\left(\frac{r}{r_w}\right)^2, \quad T_D = \frac{2\pi H \rho_c k k_{rg}(T - T_0)}{\mu_c \mu_{JTc} M_0}, \quad T_{wD} = \frac{2\pi H \rho_c k k_{rg}(T_w - T_0)}{\mu_c \mu_{JTc} M_0}, \tag{3.6a–c}$$

$$b_D = \frac{k k_{rg} M_0 b}{2\pi H \mu_c r_w}. \tag{3.7}$$

The above problem can be solved by the method of characteristics (e.g. Knobel 1999) as follows. The complete derivative of T_D with respect to ξ can be written as

$$\frac{\mathrm{d}T_D}{\mathrm{d}\tau} = \frac{\partial T_D}{\partial \tau} + \frac{\mathrm{d}\xi}{\mathrm{d}\tau}\frac{\partial T_D}{\partial \xi}. \tag{3.8}$$

Consider $\mathrm{d}\xi/\mathrm{d}\tau = 1$ such that $\xi = \tau + \xi_0$, where $\xi_0 = \xi(\tau = 0)$. By setting $\mathrm{d}\xi/\mathrm{d}\tau = 1$ and comparing to (3.3), it can then be said that

$$\frac{\mathrm{d}T_D}{\mathrm{d}\tau} = -\frac{1}{2(\tau + \xi_0)} - \frac{b_D}{(2(\tau + \xi_0))^{3/2}}. \tag{3.9}$$

Integrating (3.9) with respect to τ, applying the initial condition in (3.4) and then substituting $\xi_0 = \xi - \tau$ yields

$$T_D(\xi(\tau), \tau) = -\frac{1}{2}\ln\left(\frac{\xi}{\xi - \tau}\right) + \frac{b_D}{2^{1/2}}\left[\frac{1}{\xi^{1/2}} - \frac{1}{(\xi - \tau)^{1/2}}\right]. \tag{3.10}$$

In a similar way, the complete derivative with respect to ξ can be written as

$$\frac{\mathrm{d}T_D}{\mathrm{d}\xi} = \frac{\mathrm{d}\tau}{\mathrm{d}\xi}\frac{\partial T_D}{\partial \tau} + \frac{\partial T_D}{\partial \xi} = -\frac{1}{2\xi} - \frac{b_D}{(2\xi)^{3/2}}. \tag{3.11}$$

Integrating (3.11) with respect to ξ and applying the boundary condition in (3.4) yields

$$T_D(\xi, \tau(\xi)) = T_{wD} - \frac{1}{2}\ln(2\xi) + b_D\left[\frac{1}{(2\xi)^{1/2}} - 1\right]. \tag{3.12}$$

The two solutions are separated in the (ξ, τ) plane by the characteristic line $\tau = \xi - 1/2$. It follows that the solution for the domain defined in (3.4) is fully described by

$$T_D = \begin{cases} -\dfrac{1}{2}\ln\left(\dfrac{\xi}{\xi - \tau}\right) + \dfrac{b_D}{2^{1/2}}\left[\dfrac{1}{\xi^{1/2}} - \dfrac{1}{(\xi - \tau)^{1/2}}\right], & \xi - \tau > \dfrac{1}{2}, \\ T_{wD} - \dfrac{1}{2}\ln(2\xi) + b_D\left[\dfrac{1}{(2\xi)^{1/2}} - 1\right], & \xi - \tau \leqslant \dfrac{1}{2}. \end{cases} \tag{3.13}$$

When $b_D = 0$, (3.13) is identical to the result previously presented by Mathias *et al.* (2010), obtained by Laplace transformation and assuming Darcy's law.

3.2. *Pressure buildup*

Disregarding statements made in the previous section, following Mukhopadhyay *et al.* (2012), consider the additional assumptions that (i) the difference between the CH_4 and CO_2 properties is negligible, (ii) temperature changes are negligible and (iii) the water and rock are incompressible. The mass conservation equations reduce to

$$\theta_c \rho_c \alpha_c \frac{\partial P}{\partial t} = -\frac{1}{r}\frac{\partial}{\partial r}(r \rho_c q_c) \tag{3.14}$$

subject to the initial and boundary conditions

$$\left.\begin{array}{lll} P_I = P_0, & r_w \leqslant r \leqslant r_e, & t = 0, \\ \rho_c q_c = M_0/(2\pi H r_w), & r = r_w, & t > 0, \\ \rho_c q_c = 0, & r = r_e, & t > 0. \end{array}\right\} \tag{3.15}$$

The above PDE is nonlinear because of the dependence of ρ_c, α_c and μ_c on P. Mukhopadhyay *et al.* (2012) linearize the above equation by imposing a Pitzer correlation for the relationship between ρ_c and P. The linearized PDE is then solved in Laplace transform space and inverted back to the time domain to obtain an analytical solution for P in the form of an integral equation, which is evaluated numerically.

An arguably more simple route to solution of (3.14) is to invoke the pseudo-pressure concept of Al-Hussainy, Ramey & Crawford (1966), whereby a pseudo-pressure ψ [$\mathrm{M\,L^{-3}\,T^{-1}}$] is defined by the derivative

$$\frac{\mathrm{d}\psi}{\mathrm{d}P} = \frac{\rho_c}{\mu_c} \tag{3.16}$$

such that the Forchheimer equation, (2.4), along with (3.14) transform to

$$\frac{(\rho_c q_c)}{k k_{rg}} + \frac{b}{\mu_c}(\rho_c q_c)^2 + \frac{\partial \psi}{\partial r} = 0, \tag{3.17}$$

$$\theta_c \alpha_c \mu_c \frac{\partial \psi}{\partial t} = -\frac{1}{r}\frac{\partial}{\partial r}(r \rho_c q_c). \tag{3.18}$$

Al-Hussainy *et al.* (1966) propose that the $\alpha_c \mu_c$ term in (3.18) can be approximated as a constant based on fluid properties obtained at a pressure half-way between the minimum and maximum pressures being considered. Mukhopadhyay *et al.* (2012) identify this feature as a disadvantage. However, application of the pseudo-pressure concept in conjunction with the pseudo-time concept of Agarwal (1979) leads to a significant improvement.

Agarwal (1979) provides a pseudo-time η [–] defined by the derivative

$$\frac{\mathrm{d}\eta}{\mathrm{d}t} = \frac{1}{\alpha_c \mu_c} \tag{3.19}$$

such that (3.18) reduces to

$$\theta_c \frac{\partial \psi}{\partial \eta} = -\frac{1}{r}\frac{\partial}{\partial r}(r \rho_c q_c). \tag{3.20}$$

The relationship between ψ and P is obtained by numerically evaluating the integral

$$\psi = \int_{P_0}^{P} \frac{\rho_c}{\mu_c} \, \mathrm{d}P. \tag{3.21}$$

The relationship between η and t requires more creativity. The difficulty is that μ_c and α_c vary in both time and space. However, a good approximation for η can be obtained by assuming that P is uniform in space, such that

$$\pi H r_e^2 \theta_c \frac{\mathrm{d}\rho_c}{\mathrm{d}t} \approx M_0, \tag{3.22}$$

which on integration yields

$$\pi H r_e^2 \theta_c (\rho_c - \rho_{c0}) \approx M_0 t, \tag{3.23}$$

providing an approximate relationship between ρ_c and t. Note that $\rho_{c0} = \rho_c(P = P_0)$.

Dividing (3.19) by (3.22) leads to

$$\frac{\mathrm{d}\eta}{\mathrm{d}\rho_c} \approx \frac{\pi H r_e^2 \theta_c}{M_0 \alpha_c \mu_c}, \tag{3.24}$$

which on integration yields an approximate relationship between η and ρ_c,

$$\eta \approx \frac{\pi H r_e^2 \theta_c}{M_0} \int_{\rho_{c0}}^{\rho_c} \frac{1}{\alpha_c \mu_c} \, \mathrm{d}\rho_c. \tag{3.25}$$

Considering an identical problem but with slightly compressible fluids (e.g. Mathias *et al.* 2008; Mijic, Mathias & LaForce 2013), the analytical solution for the problem defined by the above system of equations can be written as

$$\psi - \psi_0 = \frac{M_0}{2\pi H k k_r} \left[W + \bar{b}_D r_w \left(\frac{1}{r} - \frac{16}{5 r_e} + \frac{2r}{r_e^2} - \frac{r^3}{3 r_e^4} \right) \right], \tag{3.26}$$

where

$$W = \begin{cases} \dfrac{1}{2} E_1 \left(\dfrac{\eta_e r^2}{4 \eta r_e^2} \right), & \eta_0 < \eta < 0.2423 \eta_e, \\ \dfrac{2\eta}{\eta_e} + \dfrac{r^2}{2 r_e^2} - \ln\left(\dfrac{r}{r_e} \right) - \dfrac{3}{4}, & \eta \geqslant 0.2423 \eta_e, \end{cases} \tag{3.27}$$

$$\eta_e = \frac{\theta_c r_e^2}{k k_{rg}} \tag{3.28}$$

and

$$\bar{b}_D = \frac{k k_{rg} M_0 b}{2\pi H \bar{\mu}_c r_w}, \tag{3.29}$$

where $\bar{\mu}_c$ is an estimate of an equivalent constant CO_2 viscosity and (Mathias & Todman 2010)

$$\eta_0 \approx \eta_e \left(\frac{r_w}{r_e} \right)^2 \left[\frac{(2\pi/\bar{b}_D)^2}{7 \times 10^3} + \frac{(2\pi/\bar{b}_D)^{1/2}}{3 \times 10^7} \right]^{-1}. \tag{3.30}$$

Formation thickness	$H = 150$ m
Permeability	$k = 100$ mD
Relative permeability	$k_{rg} = 0.6$
CO_2 injection rate	$M_0 = 0.3$ Mt year^{-1}
Initial pressure	$P_0 = 0.7$ MPa
Radial extent of reservoir	$r_e = 3000$ m
Well radius	$r_w = 0.1$ m
Residual water content	$\theta_w = 0.05$
Initial temperature	$T_0 = 35\,^{\circ}$C
Injection temperature	$T_w = 35\,^{\circ}$C
Volume fraction of rock	$\theta_r = 0.8$

TABLE 1. Parameter values assumed for base case.

4. Numerical solutions

Numerical solutions for the full equation were performed to explore and compare the pressure and temperature responses. Sensitivity analysis was undertaken around a base case described by the parameters given in table 1. These parameters are considered to be typical of many depleted gas reservoirs around the UK continental shelf. The constant CO_2 injection rate of 0.3 Mt year^{-1} is based on a recommendation made by Mathias *et al.* (2013*b*), following a statistical analysis of historical oil and gas production rates in the UK continental shelf. The numerical models employ a radial grid, discretized using 200 equal intervals in $\log_{10}$ space, from r_w to r_e. The Forchheimer parameter b is calculated using the correlation of Geertsma (1974):

$$b = 0.005\,\theta_g^{-5.5}(kk_{rg})^{-0.5}. \tag{4.1}$$

Simulation outputs for the aforementioned base case are presented in figure 2. The constant injection of CO_2 leads to an increase in fluid pressure. The CO_2 front pushes the methane radially outwards. Fluid pressure is greatest at the injection well. Consequently, the CO_2 expands as it moves away from the injection well and experiences lower pressures. This leads to Joule–Thomson cooling, which cools both the fluid and rock behind the front. These changing temperatures and pressures lead to increases or decreases in relevant fluid properties, which feed back to the fluid dynamics of the system.

Figure 2(*a*) shows the pressure distribution (measured at the base of the reservoir, i.e. $P + \rho_c g h_c$) at different times. Pressure conforms to a logarithmic relationship, consistent with radially symmetric problems associated with single-phase and slightly compressible fluids (e.g. Mijic *et al.* 2013). The pressure wave meets the outer boundary of the reservoir, at $r = r_e$, just after one year; the pressure is then seen to increase across the reservoir.

Figure 2(*b*) shows temperature distributions for different times. Near to the well, temperature declines with increasing distance according to a logarithmic relationship, similar to the analytical solution previously derived by Mathias *et al.* (2010). Finally, some distance away from the well, temperature recovers back to the initial temperature. The temperature decline occurs due to the expansion of the CO_2 as it migrates away from the injection well and experiences continuously decreasing pressures.

Figure 2(*c*) shows the geometry of the CO_2–CH_4 interface at different times, which takes the form of a moderately dispersed front. The dispersion is partly due to the

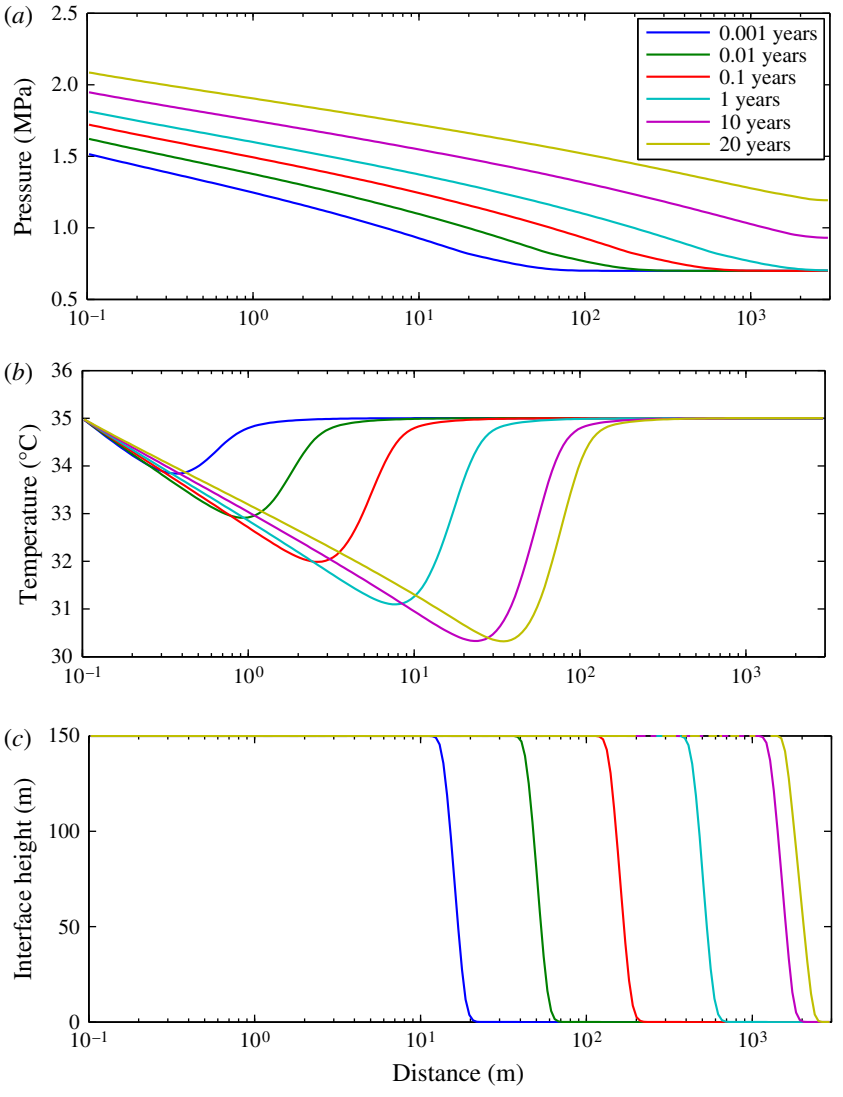

FIGURE 2. Results from the base case simulation (see table 1) including plots of: (*a*) pressure at the base of the reservoir, (*b*) temperature and (*c*) the CO_2–CH_4 interface height against radial distance for various times, as indicated in the legend.

gravity effects associated with the diffusive-like derivative of h_c in (2.11). Dispersion is also brought about due to the mobility difference between the CO_2 and CH_4 (cf. Nordbotten & Celia 2006). As discussed in § 3.1, all the changes in temperature induced by CO_2 injection reside far behind the CO_2–CH_4 interface owing to the retarding effect of the combined heat capacity of the rock, water and CO_2.

Figure 3 presents results from a sensitivity analysis around the base case described parametrically in table 1. Panels (*a*), (*c*), (*e*) and (*g*) show plots of change in bottom hole pressure in the injection well, i.e. $P(r = r_w) + \rho_c g h_c - P_0$. Panels (*b*), (*d*), (*f*) and (*h*) show plots of temperature against distance after 20 years of injection. The solid lines are from the fully coupled numerical model (hereafter referred to as

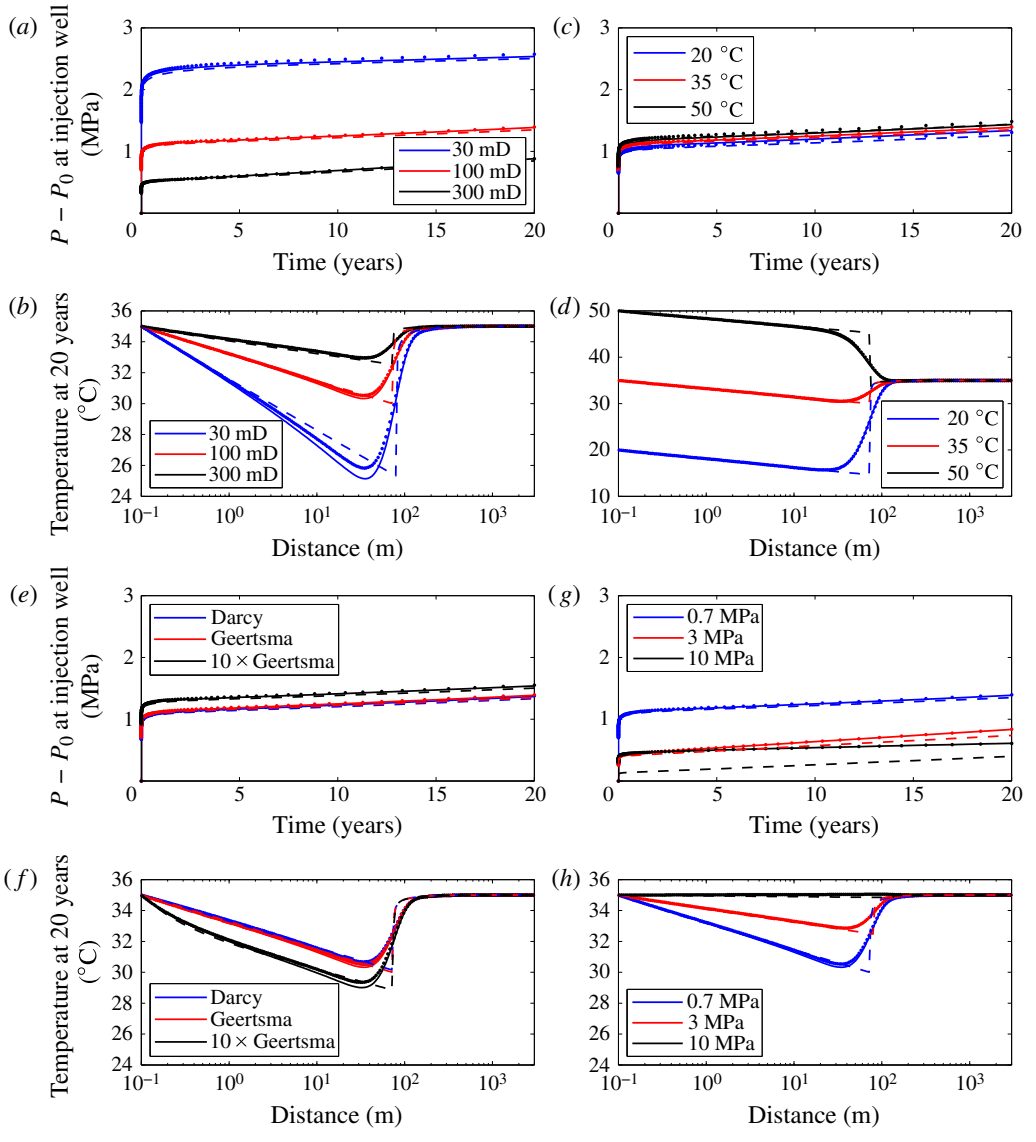

FIGURE 3. Presentation of the sensitivity analysis around the base case described in table 1 for: (*a*,*b*) permeability, (*c*,*d*) injection fluid temperature, (*e*,*f*) non-Darcy effects, and (*g*,*h*) initial pressure, as indicated in the legends. (*a*,*c*,*e*,*g*) Plots of change in bottom hole pressure against time. (*b*,*d*,*f*,*h*) Plots of temperature against radial distance after 20 years of injection. The solid, dotted and dashed lines are from the fully coupled model, a simplified isothermal model and the analytical solutions, respectively.

non-isothermal). The dotted lines are from a simplified form of the numerical model whereby all fluid properties are held constant with temperature according to the injection fluid temperature (hereafter referred to as isothermal). The dashed lines are results from the analytical solutions presented in § 3.

Figure 3(*a*,*b*) shows results looking at sensitivity to permeability. Note that an increase in permeability has a similar effect to an increase in formation thickness

and/or a decrease in injection rate. Decreasing permeability leads to increased well pressures and spatial pressure gradients. Consequently, decreasing permeability leads to increased temperature loss away from the well. Interestingly, the difference between the isothermal and non-isothermal simulation results is virtually unnoticeable, except for the estimated temperature decline associated with the 30 mD model. The difference between the models is small because the fluid properties change very little over the temperature range of 30 and 35 °C at these pressures. A more significant difference is observed for the 30 mD models, because the temperature decline is more severe.

Recall that the dashed lines are results from the analytical solutions. It is clear from figure 3(*a*) that the pseudo-pressure and pseudo-time approach is very effective at predicting the well pressures in this context, despite the fact that it ignores the CH_4 fluid properties. The heat transport analytical solution is also seen to be effective here (see figure 3*b*).

Note that previously Mathias *et al.* (2010) observed discrepancies between numerical simulation and the analytical solution (assuming Darcy flow) for temperature changes greater than 5 °C. It was argued that this was due to applying the initial pressure for calculating the constant fluid properties used. Here an estimate of the well pressure half-way through the injection period (i.e. at 10 years) is used, obtained from the aforementioned analytical solution for pressure buildup, in conjunction with the injection fluid temperature. This is found to be very effective for all the analytical solution results presented in figure 3(*b*,*d*,*f*,*h*).

Recently, Ziabaksh-Ganji & Kooi (2014) argued that a notable deficiency in the analytical solution of Mathias *et al.* (2010) (and therefore also the new solution presented in § 3.1, which uses the Forchheimer equation) was ignoring heating due to compression. Considering figure 3(*a*), it can be seen that there are initially large changes in pressure with time. But after less than a small fraction of a year, the change in pressure with time is dramatically reduced. In contrast, the large pressure changes with radial distance persist throughout the injection period (consider again figure 2*a*). Consequently, cooling due to expansion as the CO_2 moves away from the injection well has a significantly more dominant effect in this context.

Figure 3(*c*,*d*) shows results from similar simulations to those used for figure 3(*a*,*b*), except looking at sensitivity to injection fluid temperature. All model parameters were set to the values stated in table 1, except for the injection fluid temperature T_w, which was set to values shown in the legend. Note that the initial reservoir temperature was fixed at 35 °C for all the simulations. It is apparent from figure 3(*c*) that injection fluid temperature, ranging from 20 to 50 °C, has very little impact on well-pressure development. Furthermore, it is noted that again there is very little difference between results from the non-isothermal and isothermal models, and the analytical solutions are found to provide a good approximation to the well-pressure and temperature response of the system.

Figure 3(*e*,*f*) explores the importance of non-Darcy effects. Results are presented, again using the base case described by table 1, using (i) Darcy's law (i.e. $b = 0$), (ii) the Forchheimer equation with the Geertsma (1974) correlation (the base case) and (iii) a simulation with enhanced non-Darcy effects, obtained by multiplying the b parameter obtained from the Geertsma (1974) correlation by a factor of 10. There is no noticeable difference between the Darcy and Forchheimer equation models using Geertsma (1974) correlation, for both heat transport and pressure. When the non-Darcy effects are enhanced by a factor of 10, a small increase in pressure is apparent, along with a corresponding 1.5 °C temperature decline. The analytical

solutions for pressure and heat transport are found to continue to provide good approximations in this context.

The Geertsma (1974) correlation has been found to correspond to large quantities of empirical data (Mathias & Todman 2010). Multiplying the correlation by 10 represents an upper bound on likely non-Darcy effects in this porosity range. Therefore, it can be concluded that non-Darcy effects are unlikely to be a particular issue in this context. Their importance can be determined in future studies by considering the dimensionless group b_D defined in (3.7). For all the simulations presented in this paper, with the exception of the Darcy and the enhanced non-Darcy simulations, b_D was found to range from 0.07 to 0.46. The enhanced non-Darcy simulation corresponded to $b_D = 2.61$.

Originally it was hypothesized that non-Darcy effects would be important because of the low viscosity of CO_2 at the low pressures of interest. However, (2.6) shows that the significance of non-Darcy effects is also dependent on fluid density. The density of CO_2 must also therefore be sufficiently low in this context, such that non-Darcy effects are not significant here.

The final panels, figure 3(*g*,*h*), show sensitivity due to initial pressure, as indicated by the values in the legend. The change in pressure in the well is found to decrease with increasing initial pressure. This is due to the fluid density increasing with pressure, which leads to a reduction in volumetric injection rate. The temperature change is close to zero for the 10 MPa example. The temperature decline increases with decreasing initial pressure. This is due to the increased pressure gradients that occur due to the increased volumetric injection rate, combined with the increased Joule–Thomson coefficient of the CO_2 (associated with lower pressures).

The performance of the analytical solution for pressure buildup is found to reduce with increasing initial pressure. The main reason is that higher initial pressures correspond to a larger mass of residing CH_4. Consequently, the effect of ignoring CH_4 fluid properties (in the analytical solution) becomes more important. This is less of an issue with regard to the analytical solution for heat transport because temperature changes are significantly reduced at higher pressures.

Zeidouni, Nicot & Hovorka (2013) previously used the analytical solution of Mathias *et al.* (2010) to verify their non-isothermal simulations obtained using CMG's GEM. They noted that the analytical solution underestimated cooling and heating due to the neglect of brine vaporization and CO_2 dissolution, respectively. The neglect of partial miscibility (vaporization and dissolution) between the CO_2 and the residual brine represents a limitation of the numerical simulations conducted in the current study as well.

Andre *et al.* (2010) studied effects associated with partial miscibility in this context at a reservoir pressure of 15 MPa and an injection temperature of 40 °C. They found temperature variation due to vaporization and dissolution to be around 1–3 °C, respectively. Inspection of the empirical equation for the solubility limit of CO_2 in water proposed by Spycher, Pruess & Ennis-King (2003) suggests that dissolution is likely to be an order of magnitude less in the context of the low-pressure environments considered in this article. Conversely, the work of Spycher *et al.* (2003) suggests that the reduction in pressure from 15 to 0.7 MPa would lead to a doubling in the amount of water evaporated. However, evaporation of residual water around the injection well would lead to an increase in gas relative permeability. This in turn would give rise to lower pressure gradients (cf. Mathias *et al.* 2011*a*) and hence less Joule–Thomson cooling.

At this stage it is interesting to compare some of the above features with those associated with CO_2 injection into brine aquifers. For brine aquifers, the pore

space is predominantly filled with brine, which has a larger viscosity and lower compressibility than the injected CO_2. For compartmentalized aquifers, this gives rise to a significant restriction on the amount of CO_2 that can be injected, if pressures are to be constrained below fracture pressure limits (Mathias *et al.* 2013*a*). Consequently, throughout the injection duration, the vast majority of the reservoir pore space continues to be occupied by brine. Therefore, in contrast to depleted gas reservoirs, the compressibility of the injection fluid is found to have very little impact on pressure buildup (Mathias *et al.* 2011*b*). Furthermore, because of the much larger viscosity difference between the CO_2 and the brine, along with the IFT that develops between the CO_2-rich and aqueous fluid phases, the mobility difference between the injection and reservoir fluids has a much more significant impact on the pressure buildup process (Mathias *et al.* 2009, 2013*a*).

5. Summary and conclusions

In this article, a two-layer vertical equilibrium model for the injection of CO_2 into a porous reservoir containing methane and water is developed. The dependent variables solved for include pressure, temperature and CO_2–CH_4 interface height. In contrast to previous two-layer vertical equilibrium models in this context, the compressibility of all material components is fully accounted for. Non-Darcy effects are also considered, which may become important for low-viscosity fluids. With some approximations, analytic solutions for both the pressure buildup and heat transport are derived and shown to capture the main dynamics and agree well with the numerical solutions.

The results show that, for a given injection scenario, as the initial pressure in the reservoir decreases, both pressure buildup and temperature change increase. A comparison was conducted between a fully coupled non-isothermal numerical model and a simplified model where fluid properties are held constant with temperature. This simplified model was found to provide an excellent approximation when using the injection fluid temperature for calculating fluid properties, even when the injection fluid was as much as $\pm 15\,^{\circ}\mathrm{C}$ of the initial reservoir temperature. The implications are that isothermal models can be expected to provide useful estimates of pressure buildup in this context.

Non-Darcy effects were incorporated using the Forchheimer equation with the Forchheimer parameter b calculated using the Geertsma (1974) correlation. An expression for a dimensionless Forchheimer parameter b_D was provided (recall (3.7)), which can be used to assess the importance of non-Darcy effects. Non-Darcy effects are likely to be negligible providing $bD < 1$. Despite the low viscosity of CO_2 at the low pressures studied, non-Darcy effects were found to be of negligible concern throughout the sensitivity analysis undertaken. This is because the CO_2 density is also low in this context.

The analytical solution for pressure buildup, using the pseudo-pressure and pseudo-time concepts of Al-Hussainy *et al.* (1966) and Agarwal (1979), respectively, was found to provide a good approximation of the fully coupled numerical model for initial pressures $\leqslant 3$ MPa. However, for higher pressures, the approximation was less accurate. The main reason for this is that the analytical solution ignores the presence of the reservoir gas, CH_4. Larger initial reservoir pressure corresponds (for a fixed volume saturation) to a larger mass of residing CH_4, leading the CH_4 to play a more important role concerning pressure buildup.

The analytical solution for heat transport was found to be a good approximation throughout the sensitivity analysis. However, it was found to be important to apply a

sensible reference pressure and temperature for calculating the CO_2 properties. Fluid properties for this purpose were calculated using the injection fluid temperature with an estimate of well pressure half-way through the injection period, obtained using the analytical solution for pressure buildup with pseudo-pressure and pseudo-time.

Acknowledgements

This work was funded by Centrica plc and a NERC Oil and Gas Catalyst award (NE/L008076/1).

REFERENCES

AFANASYEV, A. A. 2013 Multiphase compositional modelling of CO_2 injection under subcritical conditions: the impact of dissolution and phase transitions between liquid and gaseous CO_2 on reservoir temperature. *Intl J. Greenh. Gas Control* **19**, 731–742.

AGARWAL, R. 1979 Real gas pseudo-time – a new function for pressure buildup analysis of MHF gas wells. In *SPE Annual Technical Conference and Exhibition*, SPE 8279-MS.

AL-HUSSAINY, R., RAMEY, H. J. JR. & CRAWFORD, P. B. 1966 The flow of real gases through porous media. *J. Petrol. Tech.* **577**, 363–383.

ANDRE, L., AZAROUAL, M. & MENJOZ, A. 2010 Numerical simulations of the thermal impact of supercritical CO_2 injection on chemical reactivity in a carbonate saline reservoir. *Transp. Porous Med.* **82**, 247–274.

BACHU, S. & BENNION, B. 2008*a* Effects of *in situ* conditions on relative permeability characteristics of CO_2–brine systems. *Environ. Geol.* **54**, 1707–1722.

BACHU, S. & BENNION, B. 2008*b* Interfacial tension between CO_2, freshwater, and brine in the range of pressure from (2 to 27) MPa, temperature from (20 to 125) °C, and water salinity from (0 to 334 000) mg L^{-1}. *J. Chem. Engng Data* **54**, 765–775.

BARRUFET, M., BACQUET, A. & FALCONE, G. 2010 Analysis of the storage capacity for CO_2 sequestration of a depleted gas condensate reservoir and a saline aquifer. *J. Can. Petrol. Technol.* **49**, 23–31.

BENTHAM, M. & KIRBY, M. 2005 CO_2 storage in saline aquifers. *Oil Gas Sci. Technol.* **60**, 559–567.

BUCKLEY, S. E. & LEVERETT, M. C. 1942 Mechanism of fluid displacement in sands. *Trans. AIME* **146**, 107–116.

CENGEL, Y. A. & BOLES, M. A. 2002 *Thermodynamics – An Engineering Approach*, 4th edn. McGraw-Hill.

CHEN, Z., HUAN, G. & MA, Y. 2006 *Computational Methods for Multiphase Flows in Porous Media*, Computational Science and Engineering Series, vol. 2. SIAM.

GEERTSMA, J. 1974 Estimating the coefficient of inertial resistance in fluid flow through porous media. *Soc. Petrol. Engng J.* **14**, 445–450.

GLUYAS, J. G. & HICHENS, H. M. 2003 *United Kingdom Oil and Gas Fields, Commemorative Millennium Volume*, Geological Society Memoirs, no. 20. Geological Society.

HAN, W. S., KIM, K. Y., PARK, E., MCPHERSON, B. J., LEE, S.-Y. & PARK, M.-H. 2012 Modeling of spatiotemporal thermal response to CO_2 injection in saline formations: interpretation for monitoring. *Transp. Porous Med.* **93**, 381–399.

HAN, W. S., STILLMAN, G. A., LU, M., MCPHERSON, B. J. & PARK, E. 2010 Evaluation of potential non-isothermal processes and heat transport during CO_2 sequestration. *J. Geophys. Res.* **115**, B07209.

HESSE, M. A., ORR, F. M. & TCHELEPI, H. A. 2008 Gravity currents with residual trapping. *J. Fluid Mech.* **611**, 35–60.

HESSE, M. A., TCHELEPI, H. A., CANTWELL, B. J. & ORR, F. M. JR. 2007 Gravity currents in horizontal porous layers: transition from early to late self-similarity. *J. Fluid Mech.* **577**, 363–383.

KNOBEL, R. 1999 *An Introduction to the Mathematical Theory of Waves*. American Mathematical Society.

LEMMON, E. E., MCLINDEN, M. O. & FRIEND, D. G. 2013 Thermophysical properties of fluid systems. In *NIST Chemistry WebBook*, NIST Standard Reference Database, vol. 69. National Institute of Standards and Technology, (online).

LOIZZO, M., LECAMPION, B., BERARD, T., HARICHANDRAN, A. & JAMMES, L. 2009 Reusing O&G depleted reservoirs for CO_2 storage: pros and cons. In *Offshore Europe Oil & Gas Conference & Exhibition*, SPE-124317.

MACMINN, C. W., SZULCZEWSKI, M. L. & JUANES, R. 2010 CO_2 migration in saline aquifers. Part 1. Capillary trapping under slope and groundwater flow. *J. Fluid Mech.* **662**, 329–351.

MACMINN, C. W., SZULCZEWSKI, M. L. & JUANES, R. 2011 CO_2 migration in saline aquifers. Part 2. Capillary and solubility trapping. *J. Fluid Mech.* **688**, 321–351.

MACROBERTS, D. T. 1962 Abandonment pressure of gas wells. In *SPE Petroleum Economics and Valuation Symposium*, SPE-260-MS.

MATHIAS, S. A., BUTLER, A. P. & ZHAN, H. 2008 Approximate solutions for Forchheimer flow to a well. *J. Hydraul. Engng* **134**, 1318–1325.

MATHIAS, S. A., GLUYAS, J. G., GONZÁLEZ MARTÍNEZ DE MIGUEL, G. J., BRYANT, S. L. & WILSON, D. 2013*a* On relative permeability data uncertainty and CO_2 injectivity estimation for brine aquifers. *Intl J. Greenh. Gas Control* **12**, 200–212.

MATHIAS, S. A., GLUYAS, J. G., GONZÁLEZ MARTÍNEZ DE MIGUEL, G. J. & HOSSEINI, S. A. 2011*a* Role of partial miscibility on pressure buildup due to constant rate injection of CO_2 into closed and open brine aquifers. *Water Resour. Res.* **47**, W12525.

MATHIAS, S. A., GLUYAS, J. G., GONZÁLEZ MARTÍNEZ DE MIGUEL, G. J., THATCHER, K. E. & ZIMMERMAN, R. W. 2011*b* Pressure buildup during CO_2 injection into a closed brine aquifer. *Transp. Porous Med.* **89**, 383–397.

MATHIAS, S. A., GLUYAS, J. G., MACKAY, E. J. & GOLDTHORPE, W. H. 2013*b* A statistical analysis of well production rates from UK oil and gas fields – implications for carbon capture and storage. *Intl J. Greenh. Gas Control* **19**, 510–518.

MATHIAS, S. A., GLUYAS, J. G., OLDENBURG, C. M. & TSANG, C. F. 2010 Analytical solution for Joule–Thomson cooling during CO_2 geo-sequestration in depleted oil and gas reservoirs. *Intl J. Greenh. Gas Control* **4**, 806–810.

MATHIAS, S. A., HARDISTY, P. E., TRUDELL, M. R. & ZIMMERMAN, R. W. 2009 Approximate solutions for pressure buildup during CO_2 injection in brine aquifers. *Transp. Porous Med.* **79**, 265–284.

MATHIAS, S. A. & TODMAN, L. C. 2010 Step-drawdown tests and the Forchheimer equation. *Water Resour. Res.* **46**, W07514.

MIJIC, A., MATHIAS, S. A. & LAFORCE, T. C. 2013 Multiple well systems with non-Darcy flow. *Ground Water* **51**, 588–596.

MUKHOPADHYAY, S., YANG, S. Y. & YEH, H. D. 2012 Pressure buildup during supercritical carbon dioxide injection from a partially penetrating borehole into gas reservoirs. *Transp. Porous Med.* **91**, 889–911.

NIELD, D. A. & BEJAN, A. 2006 *Convection in Porous Media*, 3rd edn. Springer.

NORDBOTTEN, J. M. & CELIA, M. A. 2006 Similarity solutions for fluid injection into confined aquifers. *J. Fluid Mech.* **561**, 307–327.

OKWANANKE, A., YEKEEN ADEBOYE, B. & SULAIMON, L. A. 2011 Evaluation and performance of natural gas storage in depleted gas reservoirs. *Petrol. Coal* **53**, 324–332.

OLDENBERG, C. M. 2007 Joule–Thomson cooling due to CO_2 injection into natural gas reservoirs. *Energy Convers. Manage.* **48**, 1808–1815.

REN, Q. Y., CHEN, G. J., YAN, W. & GUO, T. M. 2000 Interfacial tension of $(CO_2 + CH_4)$ + water from 298 K to 373 K and pressures up to 30 MPa. *J. Chem. Engng Data* **45**, 610–612.

SINGH, A. K., BAUMANN, J., HENNINGES, J., GOERKE, U. J. & KOLDITZ, O. 2012 Numerical analysis of thermal effects during carbon dioxide injection with enhanced gas recovery: a theoretical case study for the Altmark gas field. *Environ. Earth Sci.* **67**, 497–509.

SINGH, A. K., GOERKE, U. J. & KOLDITZ, O. 2011 Numerical simulation of non-isothermal compositional gas flow: application to carbon dioxide injection into gas reservoirs. *Energy* **36**, 3446–3458.

SOMERTON, W. H. 1992 *Thermal Properties and Temperature-Related Behavior of Rock/Fluid Systems*, Developments in Petroleum Science, vol. 37. Elsevier.

SOMERTON, W. H., JANAH, A. H. & ASHQAR, P. I. 1981 Thermal expansion of fluid saturated rocks under stress. In *SPWLA 22nd Annual Logging Symposium, Society of Petrophysicists and Well-Log Analysts*. SPWLA-1981-D.

SPYCHER, N., PRUESS, K. & ENNIS-KING, J. 2003 CO_2–H_2O mixtures in the geological sequestration of CO_2. I. Assessment and calculation of mutual solubilities from 12 to 100 °C and up to 600 bar. *Geochim. Cosmochim. Acta* **67**, 3015–3031.

ZEIDOUNI, M., NICOT, J. P. & HOVORKA, S. D. 2013 Monitoring above-zone temperature variations associated with CO_2 and brine leakage from a storage aquifer. *Environ. Earth Sci.* (in press).

ZENG, Z. & GRIGG, R. 2006 A criterion for non-Darcy flow in porous media. *Transp. Porous Med.* **63**, 57–69.

ZIABAKSH-GANJI, Z. & KOOI, O. 2014 Sensitivity of Joule–Thomson cooling to impure CO_2 injection in depleted gas reservoirs. *Appl. Energy* **113**, 434–451.

ZIMMERMAN, R. W. 1989 Thermal conductivity of fluid-saturated rocks. *J. Petrol. Sci. Engng* **3**, 219–227.

ZIMMERMAN, R. W. 2000 Coupling in poroelasticity and thermoelasticity. *J. Rock Mech. Min. Sci.* **37**, 79–87.